Energy Storage Materials 17 (2019) 260–265

Contents lists available at ScienceDirect

Energy Storage Materials

journal homepage: www.elsevier.com/locate/ensm

High Coulombic efficiency cathode with nitryl grafted sulfur for Li-S battery

Xuejun Liu, Tao Qian*, Jie Liu, Mengfan Wang, Hongli Chen, Chenglin Yan*

Soochow Institute for Energy and Materials Innovations, College of Energy, Collaborative Innovation Center of Suzhou Nano Science and Technology, Key Laboratory of Advanced Carbon Materials and Wearable Energy Technologies of Jiangsu Province, Soochow University, Suzhou 215006, China

ABSTRACT

The development of lithium sulfur (Li-S) batteries has provided a popular alternative to the current state-of-art battery technologies because of their low cost as well as high theoretical specific energy. However, it is still challenging to develop sulfur cathodes with high Coulombic efficiency due to the polysulfide dissolution problem. Herein, we present a new strategy to improve the Coulombic efficiency by using nitryl grafted sulfur cathode, which is confirmed by *in-situ* XRD measurement and XPS analysis. The formed SEI layer on the nitryl grafted sulfur cathode could effectively trap the soluble polysulfide and avoid polysulfide migration from cathode into electrolyte, which allows significant improvement in the capacity retention of 80.6% after 450 cycles. In addition, a Coulombic efficiency of ~ 100% is achieved for the nitryl grafted sulfur (Nitryl-S) cathode, which is superior to the value of bare S cathode. The excellent performance is owing to the significantly reduced concentration of soluble polysulfide as evidenced by *in-situ* UV/Vis spectroscopy analysis. Thus this strategy might open up a new avenue for practical application of Li-S batteries.

The extensive use of portable electronics, consumer devices as well as large-scale grid energy storage stimulates the development of high-performance and long cycle life batteries [1,2]. However, the existing lithium-ion (Li-ion) batteries exhibit limited energy density and cycle life, and it is insufficient to meet the booming requirements for personal electronics and electric vehicles. Hence, developing electrode materials with high charge capacities is urgently needed. Sulfur (S), which could theoretically achieve a high energy density of 2500 W h kg^{-1} (or 2800 W h L^{-1}) based on the stepwise conversion reaction of S_8 with Li ions, is believed to succeed the current state-of-art Li-ion batteries [3–6]. However, the full utilization of S is hard to be achieved as the remaining challenges still need to be addressed. The highly soluble polysulfide immediates could lead to the mass loss of active materials and significant capacity fading during the successive charging and discharging process [7]. Besides, the dissolved polysulfide migrates from cathode to anode and causes unfavorable side reactions with Li anode, which leads to self-discharge and low Coulombic efficiency [8].

Various routes were developed to address the polysulfide dissolution problem. Carbonaceous materials with large surface areas and pore volumes, such as hollow carbon nanosphere [9], mesoporous carbon [10], carbon nanotube [11], have been designed to encapsulate sulfur and thus prevent polysulfide from escaping into the electrolyte. Great efforts have also been made to alleviate the dissolution of sulfur by introducing a barrier layer between the cathode and separator. To restrain polysulfide diffusion, various materials including graphene [12], mesoporous carbon [13], boron nitride [14] and layered double hydroxide [15] have been used. However, further improvements are still needed.[16] In addition to the materials modification aiming at avoiding the polysulfide dissolution, reducing the side reaction with Li anode by using additives in the electrolyte to passivate the Li surface has also shown a favorable advance on the performance of Li-S battery. For example, Cui's group [17] demonstrated the effectively suppressed parasite reaction between lithium polysulfide and Li anode using lithium polysulfide (Li_2S_8) and lithium nitrate ($LiNO_3$) as the additives. Gao and co-workers [18] employed lanthanum nitrate as the electrolyte additive, which is beneficial to slow down the electrochemical dissolution/deposition reaction on Li anode for stabilizing the surface morphology of metallic Li anode in Li-S battery. Liang and co-workers [19] reported the suppressive effect of phosphorus pentasulfide (P_2S_5) on the polysulfide shuttle phenomenon. However, it is insufficient to rely solely on the use of additives to improve the performance of Li-S batteries.

In this study, we report a novel promising approach for the formation of solid electrolyte interphase (SEI) layer on sulfur cathode, which protects the sulfur cathode against polysulfide dissolution and shuttling effect. The chemical modification of element sulfur was enabled via inverse vulcanization process, during which nitryl group was introduced and chemically grafted across the sulfur matrix (Nitryl-S) (Fig. 1). Moreover, *in-situ* X-ray diffraction (XRD) measurements as well as X-ray photoelectron spectroscopy (XPS) analysis demonstrate

* Corresponding authors.
E-mail addresses: tqian@suda.edu.cn (T. Qian), c.yan@suda.edu.cn (C. Yan).

https://doi.org/10.1016/j.ensm.2018.07.009
Received 23 March 2018; Received in revised form 6 June 2018; Accepted 12 July 2018
Available online 19 July 2018

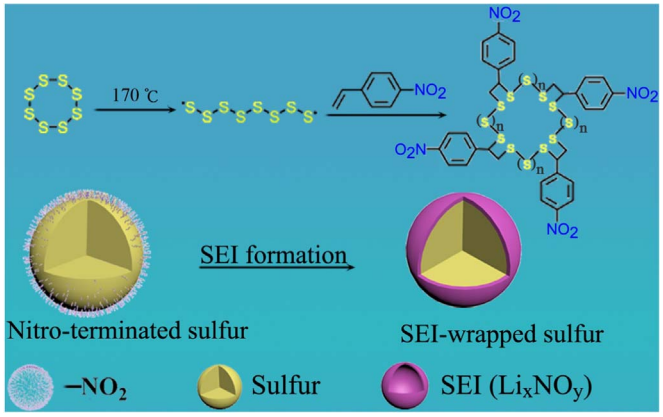

Fig. 1. The schematic illustration of the solid electrolyte interphases (SEI), which was *in-situ* formed on the sulfur particle.

that the interaction between nitryl group and Li^+ during the initial cycles allows for the formation of a very dense SEI layer. Remarkably, the Coulombic efficiency of Nitryl-S is significantly improved, maintaining nearly 100% for over 200 cycles. In order to quantitatively determine the polysulfide dissolved in the electrolyte, *in-situ* UV/Vis spectroscopy was conducted, which shows the obviously reduced concentration of the dissolved polysulfide.

For the modification of sulfur, 1-ethenyl-4-nitrobenzene was utilized and enabled the reactions with sulfur via inverse vulcanization, which allowed the covalent linkage of nitryl-end group across the sulfur matrix. The successful introduction of nitryl groups is confirmed by Fourier transform infrared spectroscopy (FT-IR) (Fig. 2A), which shows the characteristic N–O stretching (1344 and 1511 cm^{-1}) [20]. Moreover, the peaks at 992 and 920 cm^{-1}, which correspond to the characteristic bands of $-CH=CH_2$, completely disappear after the nitryl groups are covalently attached onto the sulfur matrix. Meanwhile, the stretching band at 750 cm^{-1} indicates the formation of C–S bonds [21]. In order to further investigate the surface chemical composition of the prepared sample, XPS survey was conducted and shown in Fig. 2B. The peaks appearing at 285.0, 228.2 and 164.2 eV can be assigned to C 1s and S 2s and S 2p, respectively. Another two peaks associated with N 1s and O 1s come from nitryl group modified sulfur matrix. Further confirmations are demonstrated in the high-resolution XPS spectra of C 1s and S 2p (Fig. 2C). The deconvoluted C 1s spectra shows three characteristic peaks at 284.8, 286.1, and 288.8 eV, which are arising from C-C/C=C, C-S, and C-N [21–23], respectively. The XPS spectra of S 2p exhibits the typical S-S peaks appeared at around 163.8 and 165 eV, which can be attributed to the pristine S_8. Another two peaks are located at around 161.6 and 162.7 eV, corresponding to -C-S- bonding [24]. All these results demonstrate that nitryl group has been successfully introduced on the surface of S_8. The nitryl group enables the reaction with Li^+ during the initial cycles, which allows for the formation of a very dense SEI layer. XPS analysis of Nitryl-S before cycling and after 10 cycles was carried out to illustrate the composition of SEI layer. Fig. 2D shows a comparison of the N_{1s} spectra for Nitryl-S cathode tested before and after cycling. The spectra obtained for the pristine Nitryl-S cathode exhibits the N_{1s} peak centered at 405.8 eV, which is assigned to the nitryl group. Another peak at a binding energy of 399.5 eV is associated with the transformation of the nitryl group to amino group by X-ray irradiation [25]. After 10 cycles of charge/discharge, the typical peaks for nitryl group disappears completely and the N_{1s} spectra features another two peaks at 406.7 eV and 403.2 eV that can be attributed to Li_xNO_y, which is reported as one of the common component of an SEI [26]. In addition, another peak at a

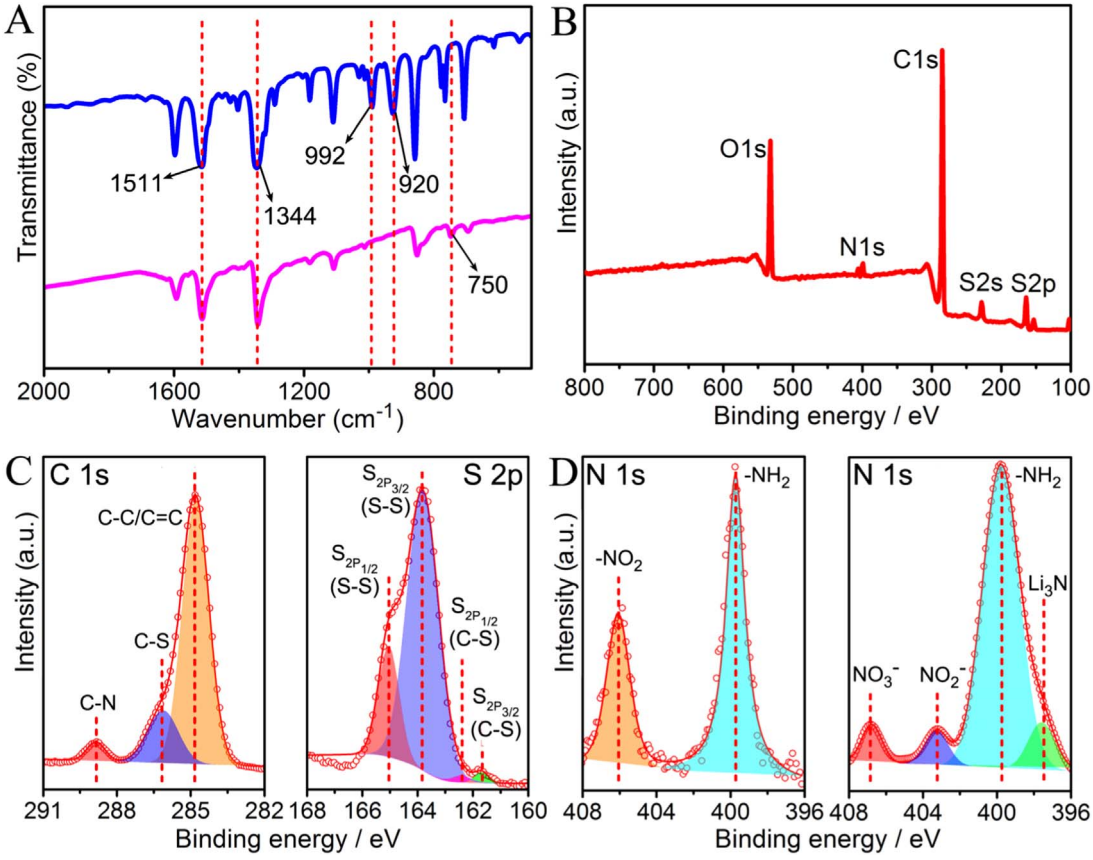

Fig. 2. (A) FT-IR spectra of 1-ethenyl-4-nitrobenzene (blue line) and Nitryl-S (pink line); (B) XPS spectra of the surface chemical composition of Nitryl-S; (C) C 1s and S 2p XPS spectra of Nitryl-S; (D) XPS analysis of Nitryl-S (left) before cycling and after 10 cycles of charge/discharge (right). (E) SEM micrographs of Nitryl-S before the electrochemical test; (F) SEM micrographs of Nitryl-S tested after 100 cycles. Inset is the corresponding TEM image after electrochemical test.

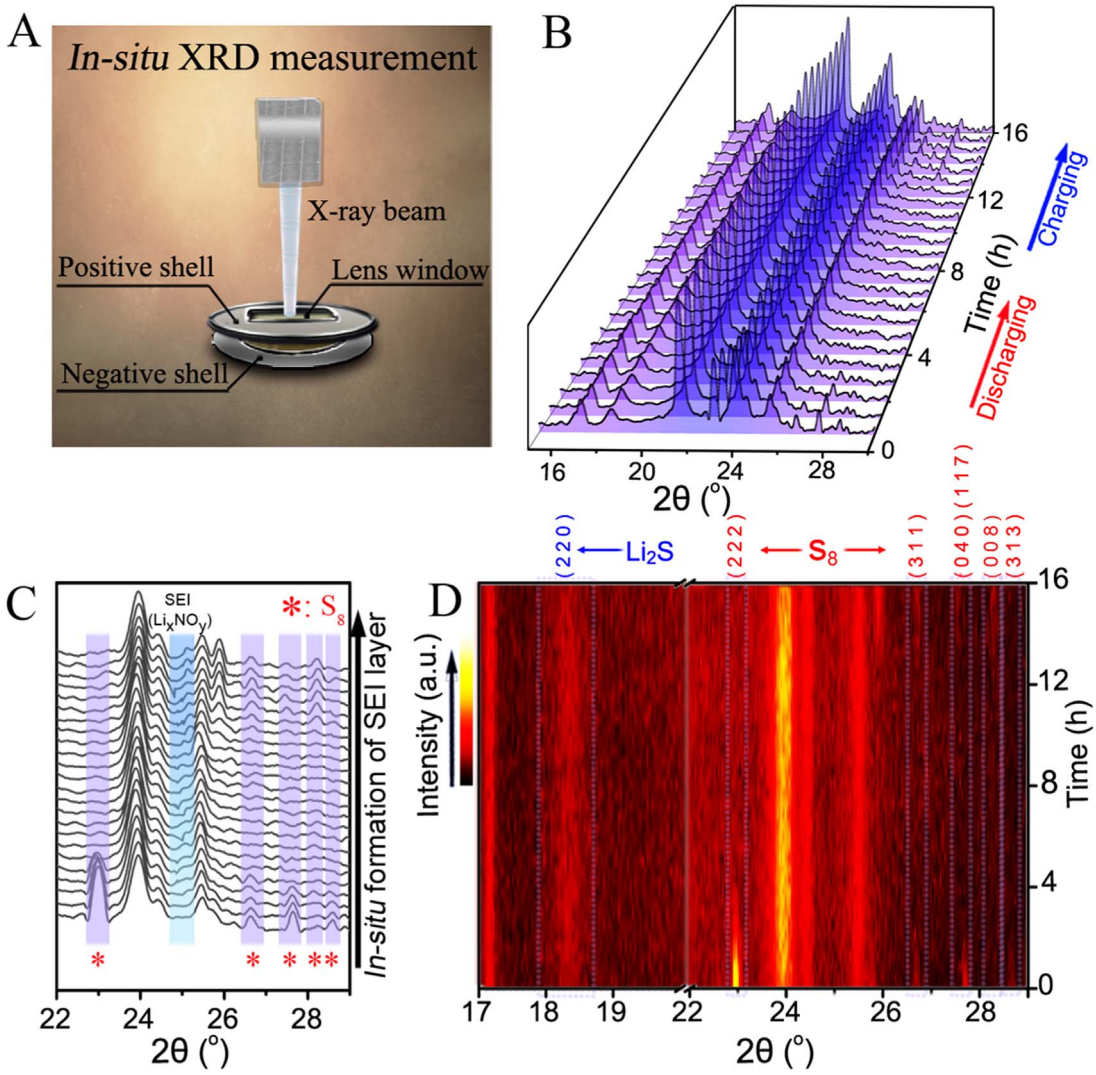

Fig. 3. (A) Schematic illustration of the cell component for *in-situ* XRD measurement; (B) *in-situ* XRD patterns evolution during initial cycle at a current rate of 0.1 C; (C) *in-situ* XRD patterns extracted from B, showing the formation of SEI layer on sulfur cathode; (D) the contour plot of *in-situ* XRD patterns collected during the initial cycle.

binding energy of 398.0 eV is associated with the formation of Li_3N, which is another main component of an SEI layer [27]. Moreover, the formation of SEI can be also confirmed by electrochemical impedance spectroscopy (EIS) measurements (Fig. S2). Before discharging, the Nyquist plot is composed of a medium-to-high frequency semicircle and a long inclined line (Warburg impedance) in the low frequency region. The high-frequency intercept on the real axis represents the ohmic resistance (R_e) of the cell, including the electrolyte and electrode resistances. The semicircle at medium-to-high frequency originates from the interface charge-transfer resistance (R_{ct}). However, after cycling two obvious semicircles can be observed. As shown in Fig. S2B, the semicircle in the high-frequency region reflects the interfacial charge transfer process, and the semicircle in the medium-frequency range is associated with the resistance of the SEI film (R_s). The fitted R_e, R_s, R_{ct} values are shown in Table S1. It is found that, after 10 cycles, the R_{ct} value of the Nitryl-S cathode decreases compared with that at the beginning, probably arising from the infiltration of the electrolyte and chemical activation process. This can be further demonstrated in Fig. 2E and F. After 100 cycles, the nitryl-S cathode maintained the similar morphology to the initial cathode due to the protective effect of SEI layer. In addition, the transmission electron microscopy (TEM) image of the resultant nitryl-S cathode (Fig. 2F) reveals the SEI layer with a thickness of ~ 5 nm is formed.

To further understand the formation mechanism of SEI layer, *in-situ* XRD was conducted. Special design of Li-S batteries enables us to realize the real-time monitoring of the local structural and chemical evolution of the nitryl-S cathode during the charge/discharge process (Fig. 3A). As shown in Fig. 3B and C, the peaks associated with (2 2 2), (3 1 1), (0 4 0), (1 1 7) and (3 1 3) [28] reveals the different crystalline planes of S_8, which decreases and finally vanish during the discharge process, indicating the sufficient reaction between S_8 and lithium ions. This can be further demonstrated by the color change presented in the contour plot of *in-situ* XRD patterns, where deep red color represents low intensity, whereas light red is for high intensity (Fig. 3D). During the discharge process, the XRD peaks of S_8 (marked by red arrow) are gradually weakened, while the peak associated with Li_2S [29] (marked by blue arrow) increases. Upon the following charging process, the intensity of Li_2S peak decreases progressively and the reappearance of S (peak (3 1 1) and (0 0 8)) towards the end of the cycle can be observed in the XRD patterns and the corresponding contour plot, demonstrating excellent electrochemical reversibility of Nitryl-S cathode. In addition, Fig. 3C shows the appearance of a completely new peak in the early stage of discharge process, and the intensity increases gradually as the charge/discharge proceeds. The new peak matches well with $LiNO_3$ (PDF#08-0466, 2θ ~ 24.7°), indicating the composition of SEI is identified to be nitrate species. This is in consistent with the N1s spectra, as discussed above, demonstrating the interaction between Li^+ and nitryl group leads to

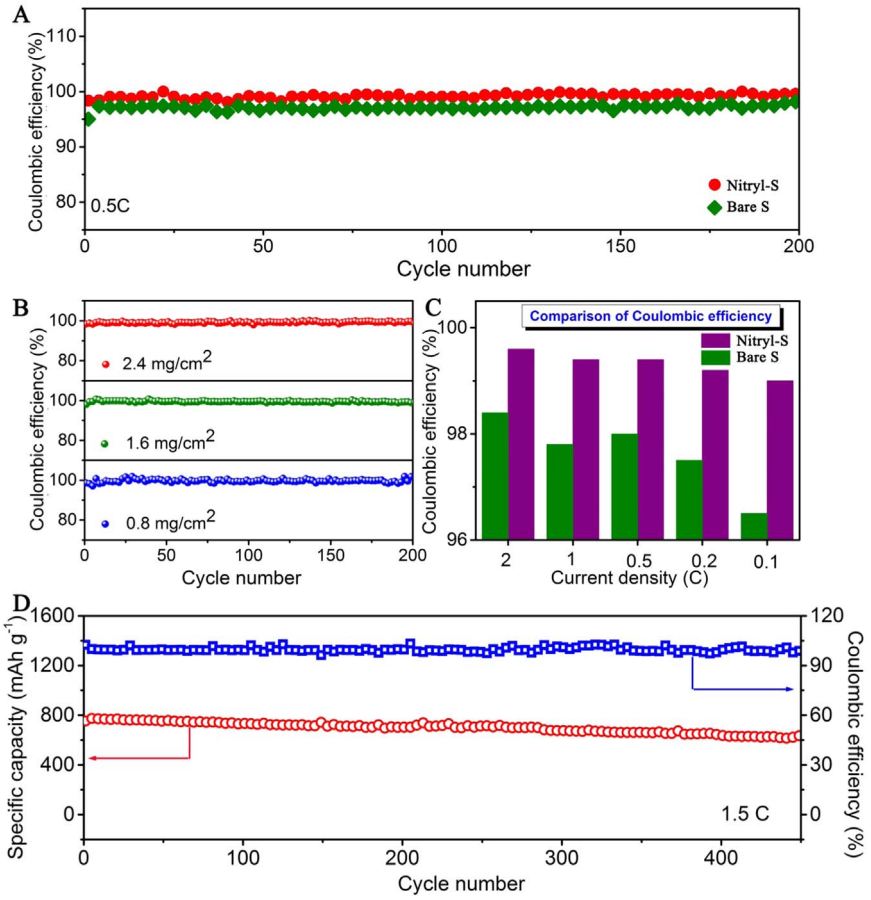

Fig. 4. (A) The Coulombic efficiencies of Nitryl-S and bare S cathodes at a current density of 0.5 C; (B) the Coulombic efficiencies of Nitryl-S with different mass loading at a current density of 0.5 C; (C) comparison of the Coulombic efficiencies for Nitryl-S and bare S tested at different current densities; (D) the long-term cycling performance and Coulombic efficiency of Nitryl-S at 1.5 C. All the measurements are conducted in the electrolyte containing 1% $LiNO_3$.

the formation of insoluble Li_xNO_y on the sulfur cathode.

The overall electrochemical properties of the Nitryl-S were studied using Nitryl-S as the cathode, and Li foil as the anode. Controlled cells were fabricated using bare S as the cathode. Fig. S3A demonstrates the cyclic voltammetry (CV) curves of Nitryl-S cathode cycled in a potential range from 1.6 to 2.9 V at a scan rate of 0.1 mV s^{-1}. Two cathodic peaks appears at approximately 2.32 and 2.03 V, representing the multistep reduction mechanism of S_8. During the following anodic scan, the peak at 2.35 V is attributed to the oxidation of lithium sulfides to sulfur. Fig. S3B demonstrates the voltage profiles of Nitryl-S cathode cycled at a current density of 1 C (1 C = 1675 mA g^{-1}) within a potential window of 1.7–2.7 V. It is obvious that after 100 cycles no apparent changes in both the shape and specific capacity could be observed, indicating the excellent cycling reversibility. This is in good agreement with CV curves as the CV curves for the successive five cycles are highly similar in both shape and size.

Although the bare S cathode has excellent electrochemical properties for potential use as positive electrodes in rechargeable Li batteries, the inevitable internal redox shuttle process limits their capacity because the sulfur reduction products, Li_xS_y species, cannot be fully re-oxidized. The *in-situ* formed SEI layer on the cathode acts as a protective layer, which could effectively trap the soluble polysulfide and avoid the shuttle effect. As shown in Fig. S4, the Nitryl-S using electrolyte containing 1 M lithium bis(trifluoromethanesulfonyl)imide (LiTFSI) in 1,3-dioxolane (DOL) and 1,2-dimethoxyethane (DME) (1/1, v/v) can operate without failure for 200 cycles with a Coulombic efficiency of ~98%, which is much higher than that of the bare S cathode. The bare S cathode could only deliver a small Coulombic efficiency of 90%, indicating the vigorous reaction between Li anode and polysulfide. Lithium nitrate ($LiNO_3$), as an effective additive, can participate in the formation of a passivation film on Li metal and protect against growth of Li dendrites, which further promotes the efficiency. When using electrolyte containing only 1 wt% $LiNO_3$, the cell based on Nitryl-S cathode maintains a high average Coulombic efficiency of ~ 100% over 200 cycles (Fig. 4A). In contrast, a relatively smaller value of 97% is obtained for bare S based cell. As a challenging factor for the commercialization of Li-S battery, the increase of the sulfur loading always leads to the reduced electrochemical performance. Fig. 4B demonstrates the Coulombic efficiency of Nitryl-S with mass loading of sulfur increases from 0.8 to 2.4 mg cm^{-2}, maintaining the similar value of ~ 100% through 200 cycles. Rate performance of Nitryl-S was evaluated at various current rates from 0.1 to 2 C. As shown in Fig. S5, the Nitryl-S cathode delivers a reversible capacity of 1169 mAh g^{-1} (0.1 C), 988 mAh g^{-1} (0.2 C), 874 mAh g^{-1} (0.5 C), 843 mAh g^{-1} (1 C), 737 mAh g^{-1} (2 C) with the average value of Coulombic efficiency over 99% respectively, which is much higher than that tested for bare S cathode (Fig. 4C). The Li-ion conductive SEI layer could only allow the effective transport of Li ions, while the penetration of electrolyte through the SEI layer is prevented. Thus the soluble polysulfide is unable to diffuse out of the compact SEI layer and trapped in the cathode. As a result, excellent capacity retention of 80.6% can be achieved for Nitryl-S after 450 cycles (Fig. 4D).

In order to get an insight into the protective effect of the SEI layer, postmortem SEM was conducted to distinguish the difference in the morphology of Nitryl-S and the bare S cathodes after cycling. Irregular precipitations on the bare sulfur cathode can be observed in Fig. S6 after 100 cycles of charge/discharge process, which is in sharp contrast to the nitryl-S cathode (Fig. 2E and F).In addition, the Li metal anode

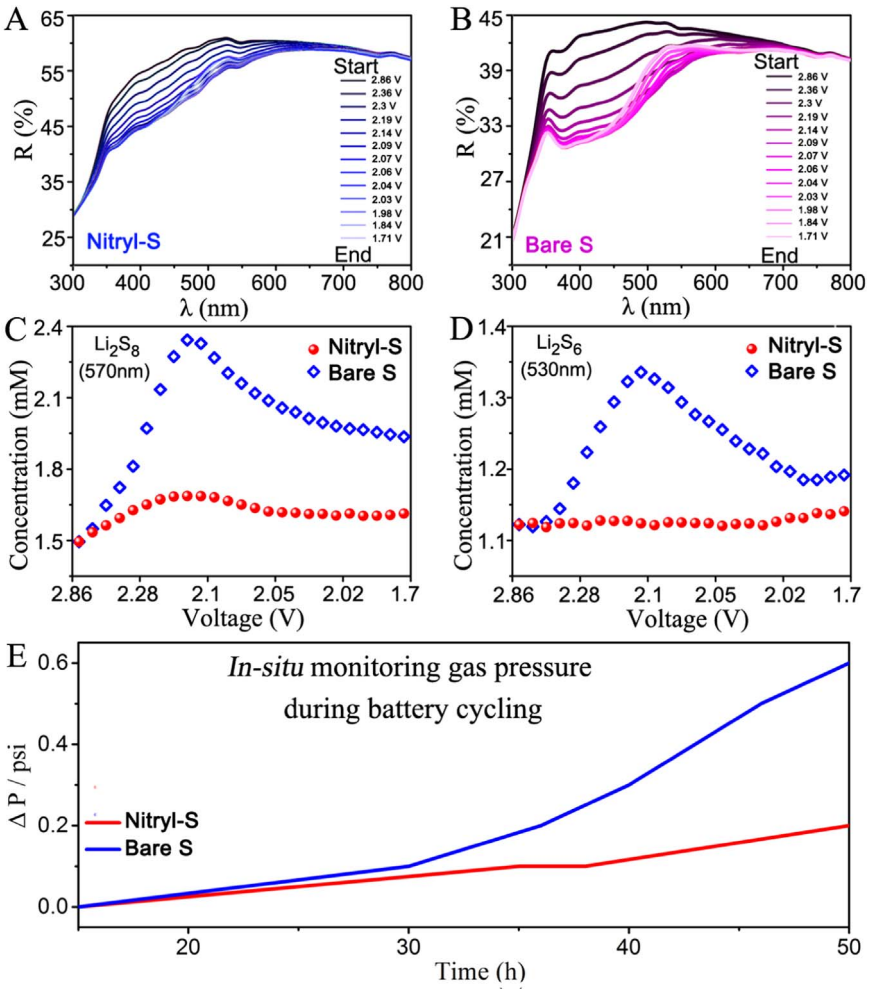

Fig. 5. *In-situ* UV/Vis spectra measured for (A) Nitryl-S, (B) Bare S: all spectra measured during discharge; (C, D) recalculated concentrations of Li_2S_8 and Li_2S_6 detected in the electrolyte; (E) *in-situ* monitoring gas pressure of the battery during cycling with Nitryl-S and bare S cathode.

with the Nitryl-S cathode shows very smooth surface, as shown in Fig. S7. On the contrary, the Li anode coupled with the bare S cathode shows a highly nonuniform morphology, related to the dendrite formation and the precipitated products. The fraction of S on the lithium metal of the Nitryl-S based cell is 3.94% from the energy dispersive spectroscopy (EDS) results, which are considerably lower than that of the traditional Li-S cell (10.46%) (Fig. S8). This implies that the *in-situ* formed SEI layer on the sulfur matrix could effectively avoid the dissolution of polysulfide into the electrolyte and subsequent precipitation on the Li anode.

In-situ UV/Vis spectroscopy was conducted to quantitatively analyze the effect of the SEI layer (Fig. 5A and B). We studied the position of the first derivatives of the UV/Vis spectra, enabling us to determine the characteristic polysulfide species during battery cycling [30,31]. It is found that the derivatives at $\lambda = 570$ and 530 nm correspond to the long-chain polysulfide of Li_2S_8 and Li_2S_6. The derivatives located at 510 nm are attributed to the mid-chain polysulfide of Li_2S_4. The derivative peaks of short-chain polysulfide is found at 450 nm. Correlations between concentrations and normalized reflectance of polysulfide (Li_2S_x, $2 \le x \le 8$) were systematically studied according to Patel's method reported previously [32,33]. From the measured spectra, the intensity of the reflection for polysulfide (Li_2S_x, $2 \le x \le 8$) at preselected wavelengths is collected and normalized, which are used to evaluate the evolvement of concentrations of different types of polysulfide according to the linear fits of the normalized intensities measured with different concentrations of the polysulfide. Fig. 5C, D and Fig. S9 shows the comparison results of the concentration changes of the lithium polysulfide in the electrolyte during the depths of discharge. It is obvious that bare S cathode shows a much higher concentration of polysulfide compared with the Nitryl-S cathode. Fewer polysulfide can be detected for the Nitryl-S cathode. These results indicate that there were few polysulfide released in the electrolyte and most of polysulfide were fixed into the electrodes by the SEI layer.

In the traditional Li-S system, gas generation always occurs due to the lithium polysulfide shuttle effect and electrolyte decomposition [34]. Fig. 5E illustrates the pressure trends during the charge/discharge process in DOL/DME using LiTFSI as the sole supporting salt. The Nitryl-S cathode displays a low and controlled gas pressure with an overall increase of 0.2 pounds per square inch (PSI), which is related to the reaction of the electrolyte with lithium, accompanied by the formation of SEI and gas evolution. The SEI layer covered on Li anode will block the further decomposition of the electrolyte. In contrast, for the bare S cathode, the pressure increases significantly by 0.6 PSI. This is because the growth of dendrites creates new anode surface area, which may further react with the electrolyte and facilitate the gassing behavior [35].

In summary, we report an original strategy of using solid electrolyte interphase (SEI) to modify sulfur through nitryl group for the enhanced Coulombic efficiency. Significantly, *in-situ* X-ray diffraction measurements allow us to clearly observe the formation process of SEI layer on sulfur cathode, which serves as polysulfide's barrier to retain sulfur active material. The SEI coated sulfur cathode thus enables a high Coulombic efficiency of ~ 99.5% at various current rates from 0.1 to 2 C (1 C = 1675 mA g^{-1}) as well as excellent capacity retention. The above

results were further proved by *in-situ* UV/Vis spectra, showing the significantly reduced concentration of soluble polysulfide.

Acknowledgements

We acknowledge the support from the National Natural Science Foundation of China (No. 51622208, No. 21703149).

Appendix A. Supporting information

Supplementary data associated with this article can be found in the online version at doi:10.1016/j.ensm.2018.07.009.

References

[1] J.M. Tarascon, M. Armand, Nature 414 (2001) 359–367.
[2] M. Armand, J.M. Tarascon, Nature 451 (2008) 652–657.
[3] Z.W. Seh, Y.M. Sun, Q.F. Zhang, Y. Cui, Chem. Soc. Rev. 45 (2016) 5605–5634.
[4] Y.X. Yin, S. Xin, Y.G. Guo, L.J. Wan, Angew. Chem. Int. Ed. 52 (2013) 13186–13200.
[5] J. Zhang, Y. Shi, Y. Ding, L.L. Peng, W.K. Zhang, G.H. Yu, Adv. Energy. Mater. 7 (2017) 1602876.
[6] J. Zhang, Y. Shi, Y. Ding, W.K. Zhang, G.H. Yu, Nano Lett. 16 (2016) 7276–7281.
[7] R. Xu, J. Lu, K. Amine, Adv. Energy Mater. 5 (2015) 1500408.
[8] N. Xu, T. Qian, X.J. Liu, J. Liu, Y. Chen, C.L. Yan, Nano Lett. 17 (2017) 538–543.
[9] C.F. Zhang, H.B. Wu, C.Z. Yuan, Z.P. Guo, X.W. Lou, Angew. Chem. 124 (2012) 9730–9733.
[10] X.L. Ji, K.T. Lee, L.F. Nazar, Nat. Mater. 8 (2009) 500–506.
[11] G.J. Hu, Z.H. Sun, C. Shi, R.P. Fang, J. Chen, P.X. Hou, C. Liu, H.M. Cheng, F. Li, Adv. Mater. 29 (2017) 1603835.
[12] G.M. Zhou, L. Li, D.W. Wang, X.Y. Shan, S.F. Pei, F. Li, H.M. Cheng, Adv. Mater. 27 (2015) 641–647.
[13] J. Balach, T. Jaumann, M. Klose, S. Oswald, J. Eckert, L. Giebeler, Adv. Funct. Mater. 25 (2015) 5285–5291.
[14] Y. Fan, Z. Yang, W.X. Hua, D. Liu, T. Tao, M.M. Rahman, W.W. Lei, S.M. Huang, Y. Chen, Adv. Energy Mater. 7 (2017) 1602380.
[15] H.J. Peng, Z.W. Zhang, J.Q. Huang, G. Zhang, J. Xie, W.T. Xu, J.L. Shi, X. Chen, X.B. Cheng, Q. Zhang, Adv. Mater. 28 (2016) 9551–9558.
[16] H. Kim, F.X. Wu, J.T. Lee, N. Nitta, H.T. Lin, M. Oschatz, W. Cho, S. Kaskel, O. Borodin, G. Yushin, Adv. Energy Mater. 5 (2015) 1401792.
[17] W.Y. Li, H.B. Yao, K. Yan, G.Y. Zheng, Z. Liang, Y.M. Chiang, Y. Cui, Nat. Commun. 6 (2015) 7436.
[18] S. Liu, G.R. Li, X.P. Gao, ACS Appl. Mater. Interfaces 8 (2016) 7783–7789.
[19] Z. Lin, Z.C. Liu, W.J. Fu, N.J. Dudney, C.D. Liang, Adv. Funct. Mater. 23 (2013) 1064–1069.
[20] M. Graglia, J. Pampel, T. Hantke, T.P. Fellinger, D. Esposito, ACS Nano 10 (2016) 4364–4371.
[21] S.N. Talapaneni, T.H. Hwang, S.H. Je, O. Buyukcakir, J.W. Choi, A. Coskun, Angew. Chem. 128 (2016) 3158–3163.
[22] Y.Q. Zhang, D.K. Ma, Y. Zhuang, X. Zhang, W. Chen, L.L. Hong, Q.X. Yan, K. Yu, S.M. Huang, J. Mater. Chem. 22 (2012) 16714–16718.
[23] Y.J. Li, J.M. Fan, M.S. Zheng, Q.F. Dong, Energy Environ. Sci. 9 (2016) 1998–2004.
[24] H. Kim, J. Lee, H. Ahn, O. Kim, M.J. Park, Nat. Commun. 6 (2015) 7278.
[25] E. Bekyarova, M.E. Itkis, P. Ramesh, C. Berger, M. Sprinkle, W.A. de Heer, R.C. Haddon, J. Am. Chem. Soc. 131 (2009) 1336–1337.
[26] D. Aurbach, E. Pollak, R. Elazari, G. Salitra, C.S. Kelley, J. Affinito, J. Electrochem. Soc. 156 (2009) A694–A702.
[27] J. Guo, Z.Y. Wen, M.F. Wu, J. Jin, Y. Liu, Electrochem. Commun. 51 (2015) 59–63.
[28] N.A. Cañas, S. Wolf, N. Wagner, K.A. Friedrich, J. Power. Sources 226 (2013) 313–319.
[29] S. Walus, C. Barchasz, R. Bouchet, J.C. Leprêtre, J.F. Colin, J.F. Martin, E. Elkaïm, C. Baehtz, F. Alloin, Adv. Energy Mater. 5 (2015) 1500165.
[30] W. Chen, T. Qian, J. Xiong, N. Xu, X.J. Liu, J. Liu, J.Q. Zhou, X.W. Shen, T.Z. Yang, Y. Chen, C.L. Yan, Adv. Mater. 29 (2017) 1605160.
[31] J. Liu, T. Qian, M.F. Wang, X.J. Liu, N. Xu, Y.Z. You, C.L. Yan, Nano Lett. 17 (2017) 5064–5070.
[32] M.U.M. Patel, R.D. Cakan, M. Morcrette, J.M. Tarascon, M. Gaberscek, R. Dominko, ChemSusChem 6 (2013) 1177–1181.
[33] M.U.M. Patel, R. Dominko, ChemSusChem 7 (2014) 2167–2175.
[34] A. Jozwiuk, B.B. Berkes, T. Weiß, H. Sommer, J. Janek, T. Brezesinski, Energy Environ. Sci. 9 (2016) 2603–2608.
[35] B.C. Yu, K. Park, J.H. Jang, J.B. Goodenough, ACS Energy Lett. 1 (2016) 633–637.